

## Article

# Tracking the Convection Potential Based on a Foundation Remote Sensing Air Sounding Profile System

Xiaomeng Lin <sup>1,2</sup>, Hong Chen <sup>1,2</sup> , Nan Zhang <sup>1,2,\*</sup> , Yinghua Wei <sup>1,2</sup>, Yiwei Liu <sup>1,2</sup> and Yanchun Wang <sup>1,2</sup>

<sup>1</sup> Tianjin Key Laboratory for Oceanic Meteorology, Tianjin 300074, China; littlelemon0526@163.com (X.L.); chenhongfengye@163.com (H.C.); weiyinghua1980@163.com (Y.W.); qxtlyw@163.com (Y.L.); wangyc23@126.com (Y.W.)

<sup>2</sup> Tianjin Meteorological Observatory, Tianjin 300074, China

\* Correspondence: nanzhangnanzhang@163.com

**Abstract:** Using ground-based remote sensing equipment (wind profile radar and microwave radiometer) data and ground automatic station data, a ground-based remote sensing sounding profile system (FAS) is constructed, which aims to make use of its advantages of high resolution, high accuracy, and low cost to make up for the lack of space–time density in existing conventional sounding layer information. The retrieval results of remote sensing sounding profiles in Beijing from May 2021 to September 2022 were tested and evaluated. The results show that the correlation coefficient between FAS and conventional sounding specific humidity is 0.89, the root–mean–square deviation is 1.53 g/kg, and the evolution trends of different data sources of convective available potential energy (CAPE) and vertical wind shear are synchronous. A case study was conducted to evaluate the effectiveness of 40 severe convective processes in the Beijing Plain area. The results show that, due to the minute-level time resolution of FAS, the retrieved convective parameters could track the evolution trend of the atmospheric state with high timeliness, dynamically describe the configuration of thermodynamic parameters, and indicate the time-varying local convective potential and instability level. Therefore, it has certain short-term forecasting significance for the occurrence time, intensity, and convection type.

**Keywords:** wind profile radar; microwave radiometer; sounding data; convective parameters



**Citation:** Lin, X.; Chen, H.; Zhang, N.; Wei, Y.; Liu, Y.; Wang, Y. Tracking the Convection Potential Based on a Foundation Remote Sensing Air Sounding Profile System. *Atmosphere* **2023**, *14*, 1117. <https://doi.org/10.3390/atmos14071117>

Academic Editor: Ferdinando Salata

Received: 23 April 2023

Revised: 22 June 2023

Accepted: 27 June 2023

Published: 5 July 2023



**Copyright:** © 2023 by the authors. Licensee MDPI, Basel, Switzerland. This article is an open access article distributed under the terms and conditions of the Creative Commons Attribution (CC BY) license (<https://creativecommons.org/licenses/by/4.0/>).

## 1. Introduction

Sounding data, which can represent the temperature, humidity structure, and dynamic properties of the atmosphere over the local area prior to the occurrence of severe convective weather, have already been considered as essential reference materials for severe weather forecasting [1]. Sounding data can be utilized to identify favorable circumstances for convection occurrence and development [2,3]. Convective parameters derived from sounding data can be used to categorize the characteristics of strong convection [4–8], thereby constructing an objective prediction model for strong convection [9]. Furthermore, sounding data can be used to pattern interpretation [10], and assimilation can improve the meso-scale numerical forecast model [11].

However, the standard radiosonde network's spatial layout is insufficient, making it difficult to capture short-term local changes in environmental factors with a detection frequency of twice a day. Simultaneously, the drift in the sounding ball reduces the regional representativeness of conventional sounding data [12,13]; thus, obtaining high-resolution data on temperature, pressure humidity, and wind by other means has become the primary way to overcome the limitations of conventional sounding data. Europe took the lead in strengthening the application of commercial aircraft observation systems (AMDAR) [14] while the China Meteorological Administration (CMA) carried out sounding with high-altitude large unmanned aerial vehicles (UAVs) [15]. The observation methods of airship-

and rocket-carried sounders have also been developed at home and abroad, but there are different degrees of different types of problems, such as the high demand for suitable environment conditions, lack of professional control, poor deployment flexibility, and high costs. Some researchers combined reanalysis data with ground automatic station data to build model temperature and humidity profiles [16,17], but reanalysis data are insufficient to describe small- and medium-scale thermal changes, and model temperature and humidity data frequently do not reflect real atmospheric conditions. The USA took the lead in developing occultation soundings to realize the construction of high-quality atmospheric observation systems, and many countries have strengthened their vertical remote sensing based on satellites in recent years [18,19]. The FY-4 satellite has been developed in China, but there are few effective samples affected by the immature inversion method [20,21]. In recent years, many researchers have focused on ground-based remote sensing detection technology with high temporal and spatial resolution and have directly constructed remote sensing temperature and humidity profiles using microwave radiometers, cloud radars, wind profile radars, and other types of detection equipment. However, due to the large errors in the humidity profiles retrieved by microwave radiometers [22,23], the wind field data retrieved by wind profile radars are frequently severely distorted or missing during precipitation, making the business applications of remote sensing temperature and humidity profiles difficult to realize.

Nonetheless, the time/space density advantage of ground-based remote sensing data cannot be ignored. Both wind profile radars and microwave radiometers can perform continuous automatic observations [24], which are useful for short-term forecasting. Microwave radiometers can provide temperature and humidity profiles from the ground to a height of 10 km [25,26], and the temperature profile correlates well with conventional sounding values [11,23]. Therefore, we tried to make use of the advantages of ground-based remote sensing data and carry out quality control pertaining to the shortcomings of the detection data to obtain effective inversion results of temperature, humidity, and wind profiles, allowing for us to capture the fine thermodynamic structure of small- and medium-sized systems. Wind profile radar inversion data obtained by the wind profile radar horizontal wind (WPR-HW) method [27] can, after quality control, still provide rapid evolution information regarding the horizontal wind field, vertical velocity field, and other factors of rainy weather [28], as well as providing the continuous and detailed change process of small- and medium-sized systems [29,30] with high reliability [31,32]. At the same time, several academics have validated the feasibility of fusing wind profile radar data with other temperature profile data to obtain atmospheric specific humidity profiles [33–39] based on the influence of specific humidity changes in turbulent scattering.

In this paper, the FAS is described by reprocessing wind profile radar data, microwave radiometer data, and ground automatic station data, with the goal of reflecting local thermal and water vapor conditions and dynamic mechanisms with high timeliness, while compensating for the low spatial and temporal resolution of conventional sounding data. The FAS inversion results in Beijing were estimated from May 2021 to September 2022, and the correctness of the inversion results was evaluated using conventional sounding data in Beijing. The FAS's application effect was assessed by selecting 40 severe convective processes in the Beijing Plain, and its operational usefulness in short-term and immediate forecasting was further investigated.

## 2. Materials and Methods

### 2.1. Selection of Instruments and Data

The foundation remote sensing air sounding profile System is built using wind profile radar power spectrum data, and its related product data, as well as microwave radiometer temperature and humidity profile data from Beijing Observatory (station 54511, 39.806° N, 116.469° E). The temperature, relative humidity, dew point temperature, and ground pressure data from the same location's national reference weather station were chosen as boundary conditions, and the conventional sounding at the same location was chosen as

the FAS comparative inspection standard. The low-mode-altitude range of the wind profile radar is 150–3630 m, with a height resolution of 120 m, and the high-mode height range is 3150–10110 m, with a height resolution of 240 m and a time resolution of 2–3 min. The microwave radiometer has a detection range of 0–10 km, with a height resolution of 25 m for 0–500 m, 50 m for 500 m–2 km, and 250 m for 2–10 km, as well as a time resolution of 2 min.

## 2.2. Specific Humidity Profile Inversion Method

Through multi-channel brightness temperature observations, microwave radiometers can indirectly obtain water vapor stratification information such as water vapor density and relative humidity [40]. However, the measurement accuracy of microwave radiometers is greatly influenced by rainy weather, and it is difficult to remove the influence of water vapor on the radiometer housing [41], meaning that humidity profile data have poor usability [42]. A relevant study has revealed that merging ground-based remote sensing data based on turbulence scattering theory can yield the atmospheric specific humidity profile [32–37]. Based on this technology, this article integrates 54,511 station wind profile radar data, microwave radiometer temperature data, and ground automated station data to obtain a vertical specific humidity profile with high time precision, laying the groundwork for FAS development.

To obtain the specific humidity profile, we should calculate Brunt–Vaisala  $N$  using Formula (1). Firstly, parameters characterizing the static stability of the atmosphere are determined. Then, we calculate turbulence dissipation rate  $\varepsilon$  using Formula (2), a parameter representing the intensity of turbulence. In the next step, we calculate atmospheric refractive index gradient  $M$  using Formula (3). In the last step, we calculate stratified specific humidity using Formulas (4) and (5). At this point, we can obtain an improved specific humidity profile.

$$N^2 = \frac{g}{T} \left( \frac{dT}{dz} + \Gamma \right) \quad (1)$$

$g = 9.8 \text{ m/s}^2$  is the gravitational acceleration,  $T$  is the layer-by-layer temperature retrieved by microwave radiometer,  $z$  is the height, and  $\Gamma = 9.8 \text{ K/km}$  is the dry adiabatic direct reduction rate of temperature.

$$\varepsilon = aN\sigma^2 \quad (2)$$

$a \approx 0.6$  and  $\sigma^2$  is the width of the velocity spectrum calculated from wind profile radar data.

$$M^2 = bC_n^2 N^2 \varepsilon^{-2/3} \quad (3)$$

where  $b$  is a dimensionless constant varying with height, with the range of 0.01–0.1, and  $C_n^2$  is the refractive index structure constant calculated from wind profile radar data.

$$B(z) = 1.65 \frac{T^2}{P} M + \frac{1}{7800} \left( \frac{dT}{dz} + \Gamma \right) \quad (4)$$

$$q(z) = \theta^2 \left\{ \int_{z_0}^z B(z) \theta^{-2} dz + \frac{q_0}{\theta_0^2} \right\} \quad (5)$$

where  $B$  is the intermediate variable,  $q$  is the specific humidity value,  $P$  is the air pressure,  $\theta$  is the potential temperature,  $Z_0$  is the initial height, and  $q_0$  and  $\theta_0$  are the initial values of the specific humidity and potential temperature provided by the automatic station.

Further investigation reveals that the boundary conditions have an effect on the vertical distribution of relative humidity, and the single control variables were set as the initial value of relative humidity at the boundary, the initial temperature, and the initial ground pressure. The experimental results show that the initial relative humidity value can roughly determine the numerical range of the entire layer of the relative humidity

profile, which can be mutually confirmed by fitting the entire layer of atmospheric water vapor content to the ground water vapor pressure [43]. The initial temperature affects the change rate of specific humidity with height, and the specific humidity profile shifts to the large-value area by about 0.15 g/kg for every 1 °C decrease in temperature. The smaller the sea-level pressure, the bigger the change rate of specific humidity with height, although its sensitivity is poorer than the initial value of temperature and humidity.

### 2.3. WPR-HW [27], Method of Horizontal Wind Inversion

Sounding data reflect not only the local temperature and humidity structure, but also the dynamic properties. Real-time and accurate horizontal wind field data are required for the construction of FAS. As wind profile radar receives both atmospheric turbulence echo and precipitation particle scattering echo during precipitation, it is difficult to extract turbulence information from the power spectrum of the superposition of the two signals, resulting in a severe lack or distortion of the horizontal wind field data displayed by wind profile radar during precipitation [44]. This means that continuous and true horizontal wind field data cannot be provided.

WPR-HW [27] collects turbulence signals for the inversion of a horizontal wind field based on the idea of wind-profile radar detection technology and the power spectrum characteristics of different kinds of weather. WPR-HW's processing object is power spectrum data. First, the number and position of peak signals in each beam's power spectrum are automatically recognized. The turbulence spectrum is then automatically recognized and retrieved from the signal spectrum of symmetrical beams based on the criteria that the turbulence spectrum is symmetrical around the east–west (north–south) beams. Finally, using the recovered turbulence spectrum and the wind synthesis method, the horizontal wind field is generated. When compared to the European Centre for Medium-Range Weather Forecasts' (ECMWF's) reanalysis data, the trustworthiness of the horizontal wind field after WPR-HW quality control is confirmed, and its timeliness and efficacy fulfill the requirements of FAS construction.

### 2.4. Construction Method of Foundation-Remote-Sensing Air-Sounding-Profile System

Three vertical profiles of temperature, humidity, and wind can be obtained using the multi-source observation data provided by ground-based remote sensing equipment and ground automatic stations. During the production process, the specific humidity profile inversion method and the WPR-HW method were used. The height range of the three vertical profiles was 0–10 km. The temperature profile was obtained by microwave radiometer inversion, and the temperature value at 0 m height was corrected by the observation value of the ground automatic station. The specific humidity profile was calculated by the specific humidity profile inversion method, the specific humidity value was converted into dew point temperature value, and the dew point temperature value at 0 m height was corrected by the observation value of the ground automatic station. The horizontal wind profile was derived using wind-profile radar inversion with the WPR-HW method, and the wind direction and speed at 0 m was adjusted using the ground automatic station observation value.

The height resolution of each element was unified by the interpolation method after acquiring the vertical profiles of temperature, humidity, and wind, and the height field and pressure field were converted [45] to create FAS. Figure 1 depicts the construction method's flow chart. The detection time disparity of observation data from multiple sources used for the same time FAS should be less than 1 min during the building process. The stratification parameters were converted into diamond 5 data format, which the Meteorological Information Comprehensive Analysis and Process System (MICAPS) recognizes. Finally, FAS visuals and data are shown using MICAPS's T log-P diagram (T-lnP).

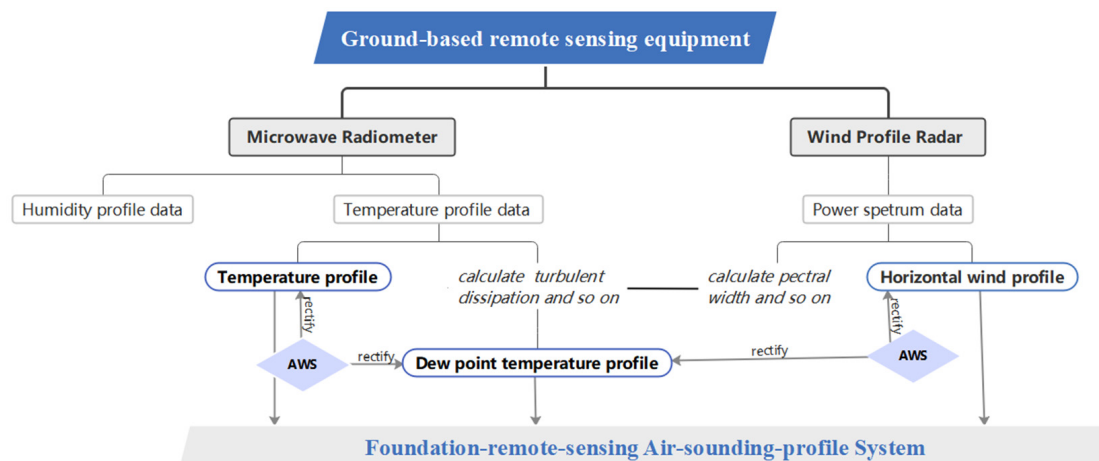


**Figure 1.** The flow chart for the construction of the foundation remote sensing air sounding system.

### 3. Method Test

The inversion findings of FAS at station 54511 from May to September in 2021–2022 were included in the database to verify the reliability of FAS. The test objects consisted of 480 specific humidity vertical profile data (40 times  $\times$  12 distance databases), 86 CAPE value data, and 40 vertical wind shear data chosen at random from the database, which contains water vapor, heat, and power information. The water vapor content in the middle and upper atmospheres was very low; the majority of the vapor was concentrated in the middle and lower tropospheres, so the specific humidity field test height ranged from the ground to 3000 m; the inspection standard was conventional sounding at the same location and at the same time, and the closest height on the database at different distances was compared. The correlation coefficient, absolute deviation, and relative deviation were all included in the test.

#### 3.1. Comparative Test of Specific Humidity Value

Figure 2a shows a scatter plot comparing FAS and conventional radiosonde-specific humidity values. When the specific humidity value is 5–10 g/kg, the overall distribution is relatively concentrated, and the distribution is relatively discrete. The correlation coefficient for 480 comparison groups is 0.89, the root mean square error is 1.53 g/kg, and the average relative deviation is 15.75%. The two data sets are highly correlated and consistent. The layer-by-layer root mean square error and average relative deviation of FAS and conventional radiosonde, respectively, are shown in Figure 2b,c, illustrating the variation trend of their deviation with height. Each layer's root mean square error is less than 2 g/kg, and the change trend with height is first growing and then reducing. The root mean square error of the ground is 1.09 g/kg, the root mean square error of 1250 m is 2 g/kg, and the root mean square error of 3000 m is 1.18 g/kg. The relative deviation of the ground is 6.76%, while the relative deviation at the height of 1250 m is 18.89%, which is similar to this finding. Because the specific wet value falls with height, the root mean square error of the height of 1250–3000 m reduces, but the relative deviation remains at 14.64–20.54%, indicating that the FAS inversion results are reliable.

The causes of the deviation are as follows. The contrast height of the two data sources must be obtained through interpolation, and there is a balloon drift problem in conventional sounding, making it difficult to obtain complete consistency in spatial positions difficult. The inversion accuracy of ground-based remote sensing data for different sky conditions must be improved. Nonetheless, the FAS-specific humidity measurement is clearly more reliable than that obtained directly by a microwave radiometer. According to a relevant study, the correlation coefficients of dew point temperature and relative humidity obtained by a microwave radiometer are 0.65–0.93 [11] and approximately 0.5 [23], respectively, when compared to traditional radiosonde. The results of the tests reveal that the FAS-

specific humidity value can reflect the vertical distribution of specific humidity in the actual atmosphere.

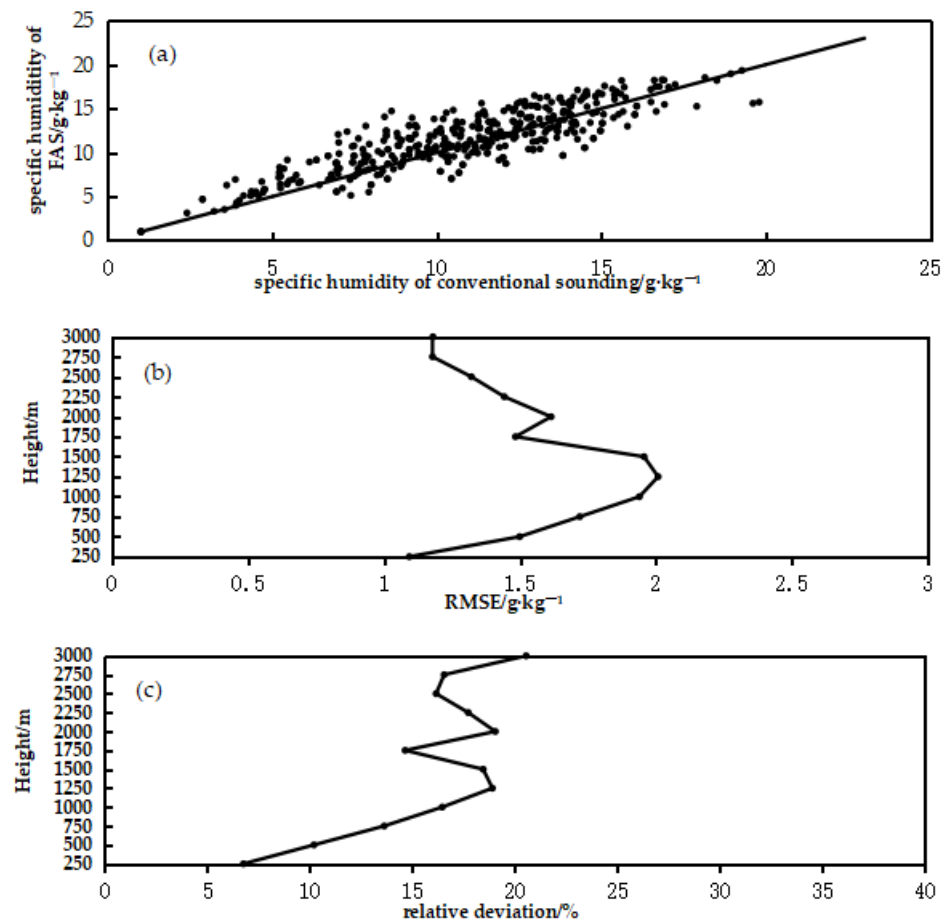


**Figure 2.** Comparison of specific humidity processed from FAS and conventional sounding (a) the scatter diagram of specific humidity, (b) the RMSE of specific humidity along with height, (c) the mean relative deviation of specific humidity along with height.

### 3.2. CAPE Value Comparison Test

Figure 3 depicts a comparison of FAS CAPE values and conventional radiosondes. It should be noted that CAPE refers to the combined action of gravity and buoyancy on the rising air block, and the integral range is from the Level of Free Convection to the Equilibrium Level. The forms of the two curves essentially correspond in the diagram, indicating a fluctuation pattern of high and low values in the same phase, and the evolution features of CAPE values of the two data sources show great synchronization. Further examination reveals that the correlation coefficient of 86 sets of comparable data is 0.81, and the average relative deviation is 33.3%, indicating that the correlation and consistency are both within a respectable range. The CAPE value is highly sensitive to variations in the temperature and humidity of the underlying surface, with a wide range of fluctuations in value. The FAS, when corrected by a ground automatic station, has an advantage compared to conventional sounding balloons that do not include interactive correction. As a result, despite the relatively substantial average absolute variance in CAPE values (309.7 J/kg), the trend of good consistency between the two forms of data is more significant to the trustworthiness of FAS CAPE parameters. The results of the tests demonstrate that the change in FAS CAPE values over time is more informative, and it can be used as a supplement to conventional sounding to compensate for the lack of temporal and spatial resolution.

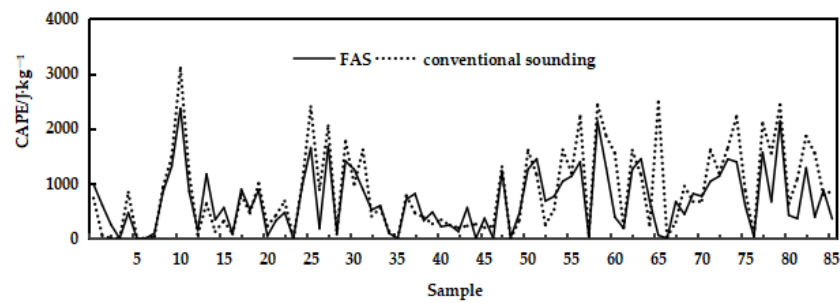


Figure 3. Comparison of CAPE processed from FAS and conventional sounding.

### 3.3. Comparative Test of Vertical Wind Shear

Figure 4a shows a comparison between FAS and conventional sounding 0–3 km vertical wind shear values. The curves of the two distinct sources have the same evolution characteristics as the CAPE value comparison curve, and the fluctuating high and low values display the same changing pattern, but the two curves intuitively exhibit a certain absolute inaccuracy. Figure 4b depicts the comparison curves of wind direction and wind speed at 3 km height between FAS and conventional sounding, and their consistency is improved when compared to 0–3 km vertical wind shear, where the correlation coefficient of wind speed is 0.92, the average absolute deviation is 1.49, the correlation coefficient of wind direction is 0.94, and the average absolute deviation is 0.36. Research has shown that the variance of 0–3 km vertical wind shear data from various sources is primarily caused by boundary conditions. The minimum detection height of the wind profile radar is 150 m, and the FAS wind field information at 0 km height originates from autonomous ground stations, so its data authenticity is higher than that of conventional sounding by remote sensing in weak wind conditions. As a result, FAS can provide dynamic field information by combining ground automatic stations with wind-profile radar data after a WPR-HW quality verification, and it can calculate effective wind vertical shear and storm helicity.

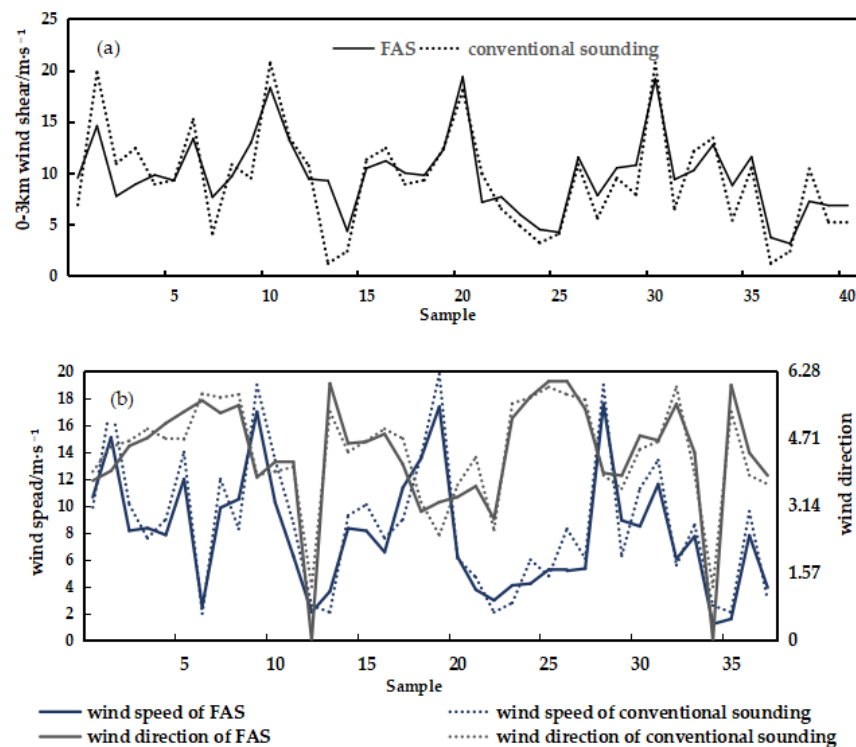


Figure 4. Comparison of dynamic field information processed from FAS and conventional sounding (a) comparison of 0–3 km wind shear, (b) comparison of wind speed and wind direction at 3 km.

## 4. Application Effect Evaluation

Using Beijing's Plain area as the research scope (the center is station 54511 and the radius is less than 40 km), 40 intense convective phenomena in 2020–2021 were chosen considering the availability of historical data, including 25 short-term heavy-precipitation processes and 15 thunderstorm processes. The FAS in the previous 8 h and the conventional sounding at the same site near the time of the powerful convective occurrences was compared and examined, as well as the application discrepancies between them. The short-term heavy rainfall on 9 June 2021 was chosen for detailed analysis, demonstrating the indicative importance of high-resolution FAS to classify and determine the potential for strong weather, as well as its ability to describe the fine thermodynamic structure of small and medium-scale systems.

### 4.1. Statistics and Analysis

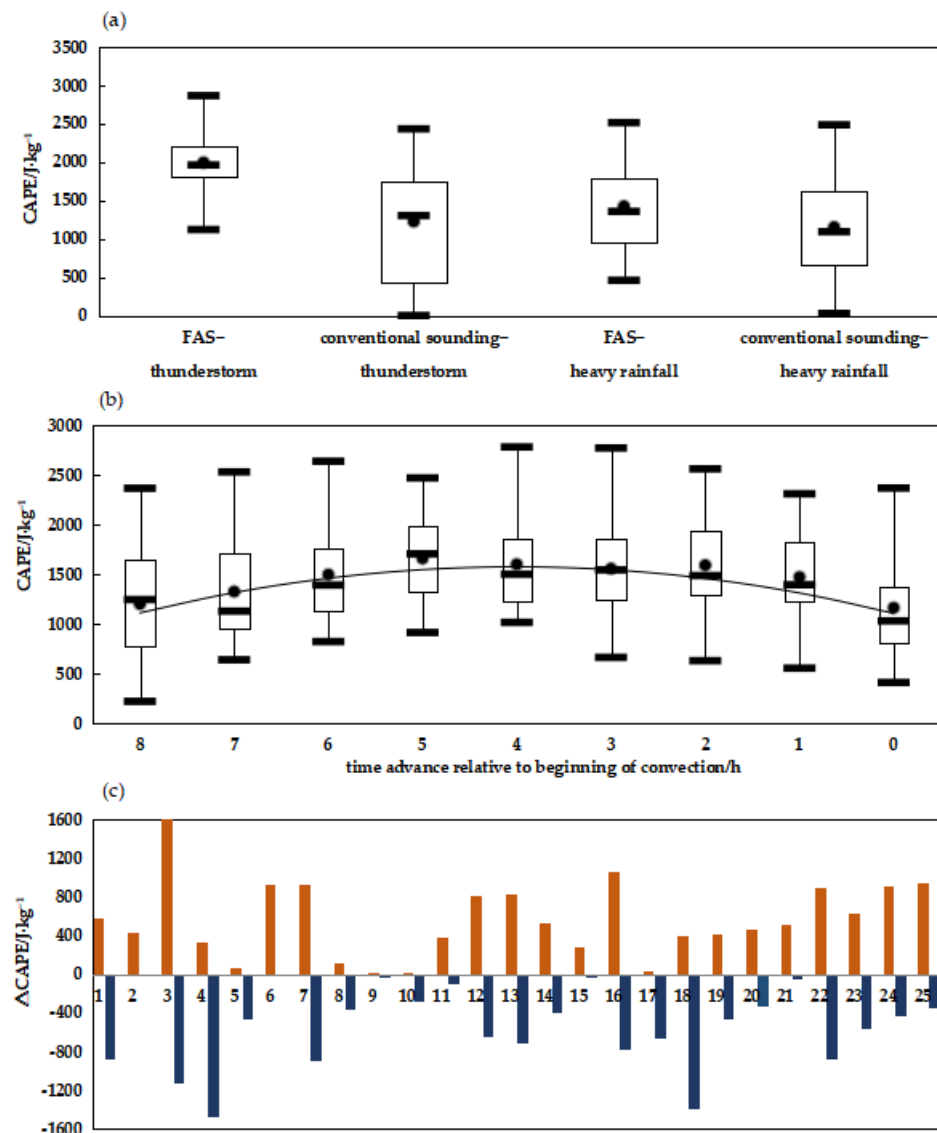
The detection time of conventional sounding was 08:00 and 20:00. Strong convection processes in Beijing frequently occur in the afternoon or evening. During the 40 occurrences, the average time difference between the occurrence of conventional sounding and the occurrence of strong convection was 6.8 h, making it difficult to capture the most unstable phase before convection. The CAPE value of conventional sounding was less than 1000 J/kg in 17 of 40 processes, with 10 processes having a CAPE value of less than 500 J/kg and two processes having a CAPE value of zero. Conventional sounding in Beijing frequently fails to represent the local convection potential in a timely manner. The FAS, on the other hand, offers the advantage of a great time resolution. The profile data with minute-level time resolution can not only reflect the local atmospheric thermal humidity state and dynamic process in real time, but also continuously observe the process of energy growth, maintenance, and release, the formation process of thermodynamic instability, and the change process of water vapor, all of which are of direct importance to the potential for and types of severe weather.

The statistics of the convective parameters CAPE, lifting index (LI), vertical wind shear, and precipitable water (PW) are presented in the form of box charts, column charts, and pie charts in this paper, the coincidence degree between the convective parameters of FAS and conventional sounding was compared with the strong convection, and the evolution law of the minute convective parameters of FAS inversion with time before the strong convection occurs was analyzed. The two ends of the box chart's line segment reflect the maximum and minimum values, the horizontal lines of the upper, middle, and lower parts of the box represent the first quartile, the second quartile, and the third quartile respectively, and the dots represent the average value.

#### 4.1.1. The Most Important Index of Convection Potential—CAPE

Figure 5a is a box diagram depicting the maximal CAPE value of FAS every 10 min within 8 h prior to the occurrence of thunderstorm gales and short-term heavy precipitation, as well as the distribution range of the CAPE value of conventional sounding at the approaching time. In general, because of the difference in observation time, the CAPE value of FAS is greater than that of conventional sounding, and the value distribution is more concentrated, allowing for it to capture the most opportune moment for convection potential. The minimal CAPE value in conventional sounding is zero, which diminishes the effect of predicting the occurrence of severe weather based on the convective potential reflected by sounding. The minimum value of CAPE in FAS is greater than 500 J/kg prior to short-term heavy precipitation and greater than 1000 J/kg prior to thunderstorms, which satisfies the business requirements for monitoring the trends in convective potential. The empirical threshold verifies that the CAPE of FAS more clearly indicates that the energy accumulation prior to thunderstorms is greater than that of short-term heavy precipitation.





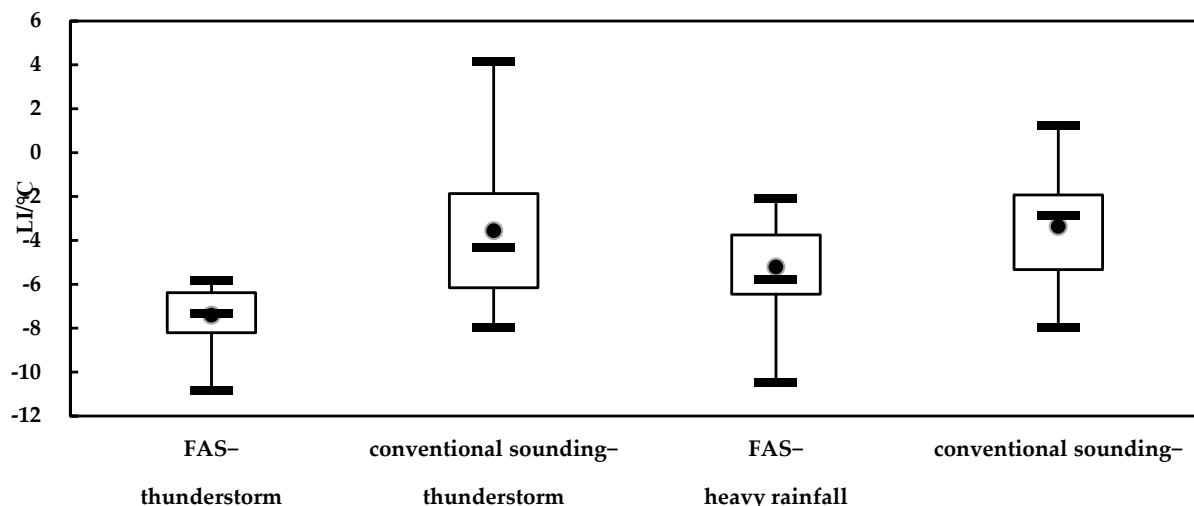
**Figure 5.** Statistics and analysis the characteristics of CAPE value in severe convective weather (a) comparison of CAPE value box plots processed using FAS and conventional sounding, (b) CAPE distribution box plots from FAS along with time in thunderstorm weather, (c) CAPE fluctuations from FAS in short-term heavy rainfall weather.

Figure 5b is a box plot depicting the hourly distribution of the CAPE value range of FAS in the eight hours preceding the thunderstorm. On average, unstable energy tends to accumulate and then release: the average period of CAPE growth is 5–8 h prior to convection, with an average increase of 458.2 J/kg. The average maximal value of CAPE is 1658.17 J/kg and occurs from 2 to 5 h before convection; this describes the brewing process of severe weather. The average duration of rapid release of CAPE is 1–2 h prior to convection, and the combination of the favorable convective potential and rapid release of CAPE has a significant impact on the occurrence of severe weather. In contrast to thunderstorms, short-term heavy precipitation is frequently accompanied by the addition of low-level water vapor, and the average downward trend of CAPE value prior to convection is obscured by the humidification of low levels in different processes and at different periods. Figure 5c presents a histogram of the variation in CAPE value before short-term intense rainfall for various processes. Although the overall fluctuation trend of CAPE value over time cannot be presented, the energy accumulation (red column)

and release (blue column) in successive processes prior to convection can be presented to varying degrees.

#### 4.1.2. Thermal Instability Index-LI

The uplift index LI measures the thermal stability of atmospheric stratification; the larger the negative value, the more unstable it is. Figure 6 is a box diagram displaying the minimum LI value of FAS every 10 min within 8 h of the occurrence of thunderstorm and short-term heavy precipitation, as well as the range distribution of LI value of conventional sounding at the approaching time. Consistent with the statistical results of CAPE value, the LI value of FAS is lower than that of conventional sounding, and the distribution of the value range is more condensed. This can correctly capture the most unstable moment of thermal power. The greatest LI values in conventional radiosondes are all positive, which influences the convection potential judged according to the thermal stability reflected by radiosondes. The greatest LI values of FAS are all smaller than  $-2\text{ }^{\circ}\text{C}$ , indicating thermal instability before convection. The LI value of FAS more clearly indicates that thermal instability prior to thunderstorm is greater than that of short-term heavy precipitation, which is mutually verified by the empirical threshold.



**Figure 6.** Statistics and analysis of the characteristics of LI value box plots from FAS and conventional sounding in severe convective weather.

#### 4.1.3. Dynamic Instability Index Vertical Wind Shear

The key to the development and maintenance of convection is dynamic stability. Dynamic instability is especially crucial in the process of severe convection nearing prediction. The amplification of vertical wind shear under particular forms of thermal instability will lead to the subsequent enhancement and development of storms. Figure 7 is a box diagram displaying the highest vertical wind shear value of FAS at 0–1 km and 0–3 km every 10 min for the 8 h preceding the thunderstorm gale, as well as the range distribution of vertical wind shear value of conventional sounding at the approaching time. Similarly, regardless of the vertical wind shear of 0–1 km or 0–3 km, the FAS inversion value is higher than that of conventional sounding, which objectively indicates the greatest dynamic instability in the convection process. The statistical value is more theoretical than conventional sounding because the value range of FAS in 0–1 km vertical wind shear is 5.44–10.65 m/s while the value range of Fas in 0–3 km vertical wind shear is 11.58–18.51 m/s.

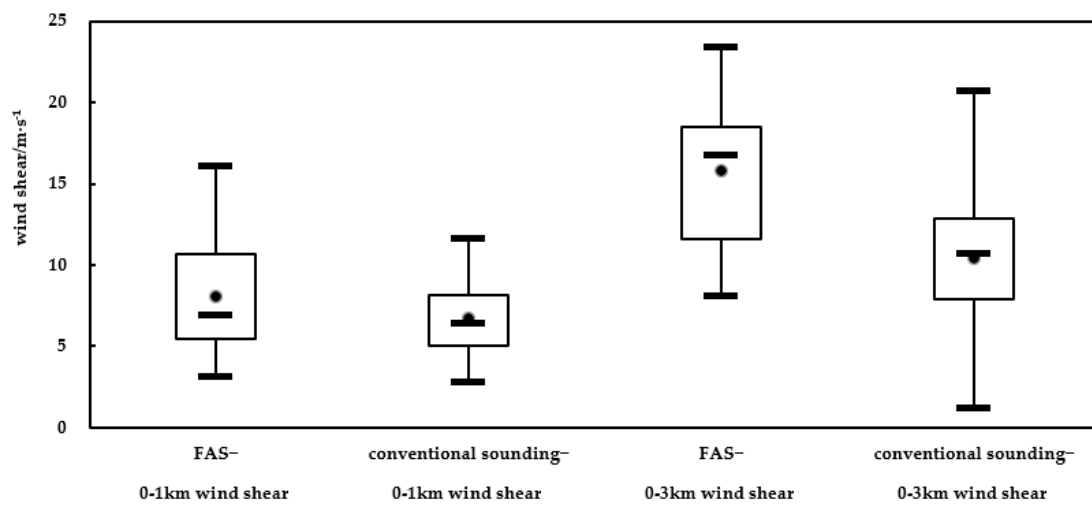


**Figure 7.** Statistics and analysis of the characteristics of wind shear box plots from FAS and conventional sounding in thunderstorm weather.

#### 4.1.4. Water-Vapor Generation and Dissipation Index–Atmospheric Precipitable Water

The FAS specific humidity profile can be used to calculate the minute-level atmospheric precipitable water, and the water-vapor growth process reflected by the atmospheric precipitable water can, to some extent, reflect the local water vapor convergence and the establishment process of low-altitude water-vapor channels. The evolution curve of the average atmospheric precipitable water recovered by FAS every 10 min within 8 h before short-term heavy precipitation is shown in Figure 8a, and displays a variable growth trend with an average rise of 8.34 mm. Figure 8b,c show pie charts showing the total increase and growth rate of atmospheric precipitable water recovered by FAS prior to the occurrence of short-term heavy rainfall. The numbers on the pie chart in Figure 8b,c represent the number of samples corresponding to the range. The fraction of total increments is 0–5 mm, 48%, 5–10 mm, 48%, 20–40%, and 32%, respectively. According to relevant research, there is a positive correlation between the incremental peak value of the entire layer of precipitable water and the peak value of rainfall intensity, and the minute-level atmospheric precipitable water product retrieved by FAS has some forecasting significance for the occurrence time and precipitation level of short-term heavy precipitation.

#### 4.2. Short-Term Heavy Precipitation Process on 9 June 2021

On 9 June 2021, the vortex caused a continuous precipitation process in Beijing Plain Area from day to night, and a short-term heavy precipitation process occurred at numerous stations in Beijing's Tongzhou District from 17:00 to 18:00. The maximum rainfall intensity was 68.3 mm, 34 km away from station 54511. Figure 9a is a radiosonde map of Beijing at 8:00 a.m. The precipitation-affected CAPE value is 194 J/kg, indicating that there is no clear convection potential and that the rise in weather scale is difficult to use as the trigger mechanism of intense convection. The southwest airflow in front of the middle–lower trough and the easterly airflow in the boundary layer constantly supplement water vapor and energy to the plain area, whereas the unfavorable condition is that the continuous ground-temperature increase is low due to precipitation. Convective characteristics with a high time resolution are a crucial basis for estimating convection potential in short-term and immediate forecasting; however, conventional radiosondes' limited observation frequency cannot match the observation needs of constantly changing convective parameters.

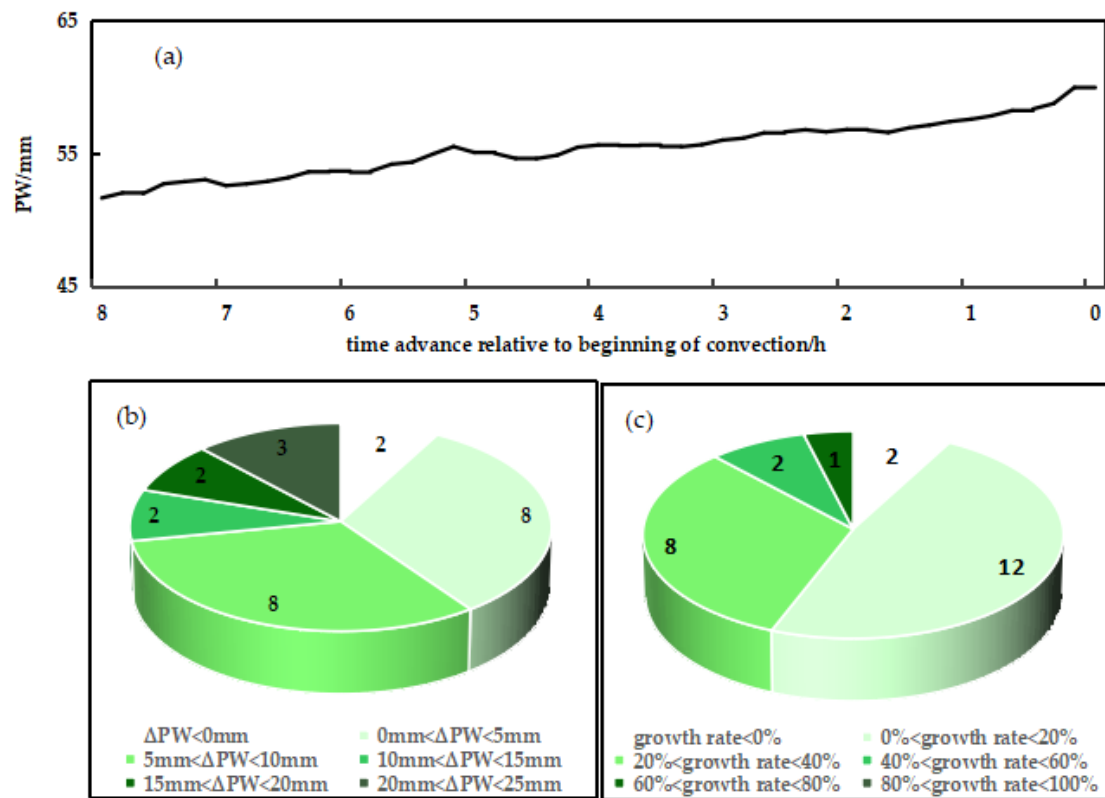


**Figure 8.** Statistics and analysis the characteristics of PW growth in short-term heavy rainfall weather (a) average growth curve along with time before short-term heavy rainfall, (b) pie chart of PW growth, (c) pie chart of PW growth rate.

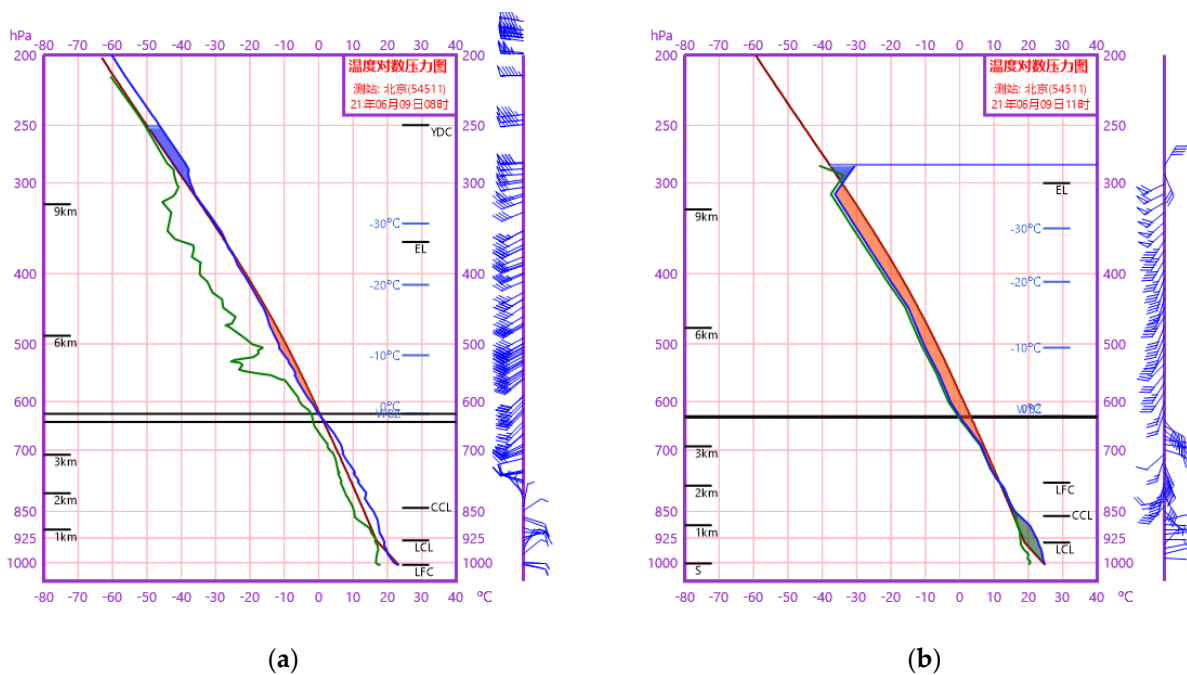


**Figure 9.** Cont.

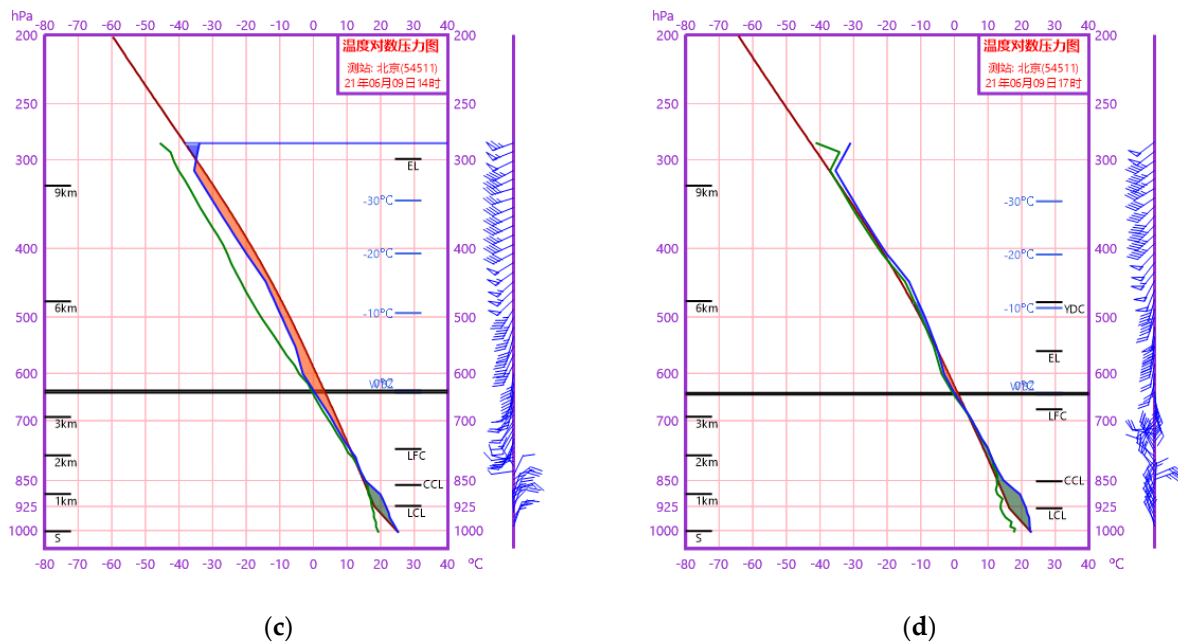


**Figure 9.** (a) T–LnP based on conventional sounding at 0800 BT on 9 June 2021, T–LnP based on FAS on 9 June 2021 (b) at 1100 BT, (c) at 1400 BT, (d) at 1700 BT. The blue line is the temperature stratification curve, the green line is the dew point temperature curve, and the brown line is the state curve.

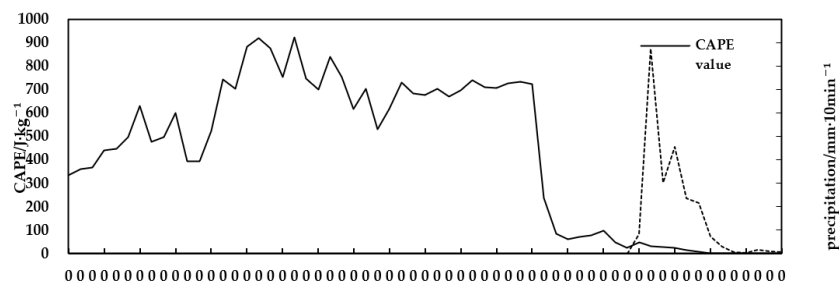
With a high time resolution, FAS can indicate the alterations in environmental parameters. Figure 9b–d presents FAS diagrams at 11:00, 14:00, and 17:00, respectively, with corresponding CAPE values of 920.4 J/kg, 703.4 J/kg, and 48.8 J/kg. The inversion data can quantify the process of CAPE’s rapid accumulation, maintenance, and release. The comparison between the Beijing radiosonde at 08:00 and the FAS at 11:00 is presented in Table 1. The highly effective convective parameters not only describe the increase in CAPE value, but also indicate that convective parameters such as k-index (K), Showalter index (SI), and integral of specific humidity for the whole layer (IQ) develop in varying degrees toward a trend of greater convection potential. The rapid growth in IQ is a result of the transport of local water vapor, which supplies sufficient water vapor sources for the occurrence of short-term heavy precipitation. At 11:00 and 14:00 UTC, the FAS has the characteristics of a high dew point in the lower layer, a high relative humidity throughout the entire layer, a close but slightly higher than the wet adiabatic direct reduction rate, and a long and narrow CAPE, and the sounding environment it depicts is typical of short-term heavy rainfall.

**Table 1.** Comparison of convective parameters processed from conventional sounding at 0800 BT and FAS at 1100 BT on 9 June 2021.

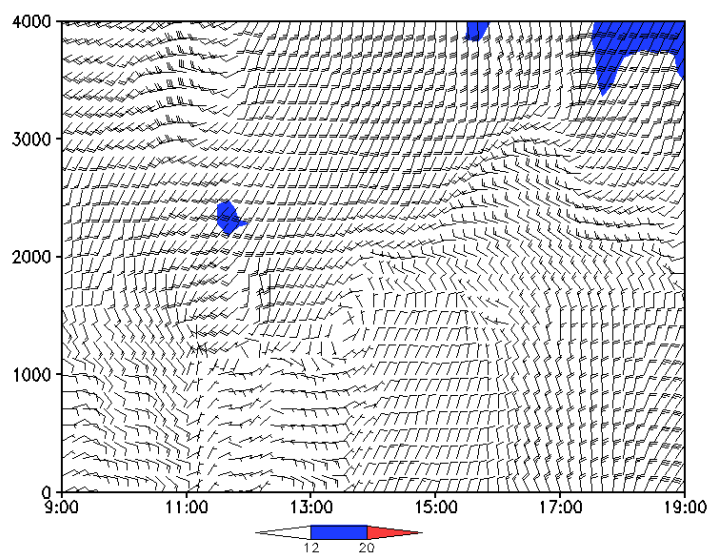
Convective Parameters	Conventional Sounding at 0800 BT	FAS at 1100 BT
CAPE	194 J·kg <sup>-1</sup>	921.9 J·kg <sup>-1</sup>
K	34.1	39.1
SI	−0.88 °C	−3.02 °C
IQ	3846.4 g·hPa·kg <sup>-1</sup>	4659.4 g·hPa·kg <sup>-1</sup>

Before strong convection, FAS is used to evaluate the relationship between the dynamic field and the ambient field. Figure 10a depicts the CAPE value calculated using FAS at station 54511 from 9:00 to 19:00, as well as the time–height profile of the horizontal wind field (WPR-HW technique) obtained from the station 54511 from 9:00 to 19:00. The energy rose and the CAPE value increased by more than 600 J/kg between 9:00 and 11:30.

The addition of humidity in the lower layer is more favourable to the CAPE value than temperature growth under the action of the southwest wind in the middle and lower layers and the southeast wind from the east to the southeast of the boundary layer. The energy maintenance stage lasts from 11:30 to 15:30, with the CAPE value ranging between 600 and 900 J/kg. Although there is little cold air disturbance during this period, the rising motion generated by the convergence of a weak wind field creates an energy value fluctuation. Because the easterly boundary layer wind overlaps the southwest wind in the intermediate and lower layers, the high-humidity and high-energy conditions are maintained by a constant supplement of warm and humid airflow. The energy-release stage lasts from 15:30 to 17:00, and a meso-scale cold air mass is jammed around 15:30. Under the action of power transmission, the invading northwest wind constantly penetrates lower and produces convergence with the southwest and easterly winds, respectively, becoming the trigger mechanism for unstable energy. The quick release of energy causes a rapid fall in CAPE value, which changes from 722.3 J/kg to 61.9 J/kg in the period from 15:30 to 16:00. The discharge of unstable energy signals a strong upward trend at the small and medium scales. A short-term heavy-precipitation process occurred at numerous stations around station 54511 at 17:00 due to environmental factors such as good humidity conditions in the middle and lower layers of the whole layer and deep warm clouds. Figure 10a shows that when the CAPE value rapidly decreased, the intensity of the downpour rapidly increased, and the time interval between energy release and heavy weather based on FAS was 1 h 30 min, which was a forecast and early warning advance.



(a)



(b)

**Figure 10.** Retrieved products utilized of ground-based remote sensing data at 54511 and observed precipitation and in AWS on 9 June 2021 (a) sequence chart of CAPE and precipitation during 0900–1900 BT, (b) time-altitude section of horizontal wind field during 0900–1900 BT.

The case of severe weather demonstrates that FAS can accurately reflect the changing trend of thermodynamically related physical quantities in real-time, and has a favorable convective potential paired with the quick release of CAPE, which can predict the occurrence of severe weather. Subjective severe weather classification results have been shown to be in good accordance with weather occurrences. At the same time, FAS can represent the interaction between environmental temperature and humidity conditions and the dynamic field, which is not only the process of energy generation and maintenance, but also the trigger mechanism of instability, and the release of energy further influences the dynamic field.

## 5. Conclusions

The foundation remote sensing air sounding profile system was built in this paper using ground-based remote sensing equipment data combined with ground automatic station data, and the mode test and case effect evaluation of FAS inversion data were performed. The following conclusions are drawn:

1. The specific humidity, CAPE, and vertical wind shear values of FAS are consistent with those of conventional sounding. The correlation coefficient of 480 contrast data groups connected to a given humidity profile is 0.89, the root mean square error is 1.53 g/kg, and the average relative deviation is 15.75%. The correlation coefficient between 86 sets of contrast data and CAPE value is 0.81, with an average relative variation of 33.33%. CAPE value evolution features from two different sources are highly synchronized. The variation in high and low values in 40 sets of comparison data related to vertical wind shear demonstrated the same tendency, and the correlation coefficients of wind speed and direction at 3 km height were 0.92 and 0.94, confirming the dependability of FAS data.
2. The FAS can perform complimentary observations with conventional sounding. The average time interval between the occurrence time of conventional sounding and the occurrence time of strong convection in 40 strong convective processes is 6.8 h, and the CAPE value of 10 processes is less than 500 J/kg, which cannot indicate the local convective potential in the afternoon or evening. The FAS has minute-level time resolution, can precisely capture the most favorable moment of convective potential, and has a high degree of agreement with the actual conditions of strong convection.
3. The FAS has a high practical utility in short-term weather forecast. Through the setup of high-frequency changeable convective parameters, the existence of convective potential and the classification of severe weather can be determined in time. The interaction between the dynamic field and the ambient field before convection occurs was examined by capturing the fine thermodynamic structure of small and medium-scale systems, which is important for improving the refinement level of short-term and imminent predictions.

FAS still has certain limitations in corporate applications. Under different weather conditions, there are varying degrees of observation errors in microwave-radiometer-temperature detection data. The CAPE inversion value of ground-based remote sensing equipment is less than the true value when the equilibrium height is high due to detection height limitations. The quality management of remote sensing data, as well as the enhancement and optimization of inversion methods, contribute to the advancement of FAS, resulting in more practical and accurate reference materials for forecasting and early warning operations.

**Author Contributions:** Conceptualization, X.L. and H.C.; methodology, X.L. and N.Z.; resources, X.L. and Y.W. (Yinghua Wei); writing—original draft, X.L. and N.Z.; writing—review and editing, X.L. and Y.W. (Yinghua Wei); supervision: Y.L., Y.W. (Yinghua Wei) and Y.W. (Yanchun Wang). All authors have read and agreed to the published version of the manuscript.

**Funding:** This research was funded by Weather forecast recovery project of China Meteorological Administration (Grant No.FPZJ2023-009, Grant No.FPZJ2023-005).

**Institutional Review Board Statement:** Ethical review and approval were waived for this study because this study is only related to meteorology and remote sensing knowledge, and has nothing to do with ethics.

**Informed Consent Statement:** The study did not involve humans.

**Data Availability Statement:** The data used in this paper are all real data in the field of atmospheric exploration, and the confidentiality is not strong. However, due to the large amount of data, data upload was not carried out. It should be noted that the article ensures the true origin of the probed data.

**Acknowledgments:** Thanks for the experimental data provided by the CMA Meteorological Observation Center, Beijing Meteorological Observation Center. Special thanks to Meng Wang from National Meteorological Centre perfecting the language of this article in her busy work. Because of her help, the article can be more fluent and organized.

**Conflicts of Interest:** The authors declare no conflict of interest.

## References

1. Wei, D.; Sun, J.S.; Lei, L. Comparative Analysis of Three Kinds of Sounding Data in the Application of the Severe Convective Weather. *J. Meteorol. Mon.* **2011**, *37*, 412–422.
2. Ye, D.Z. Application of radiosonde data. *Meteorol. Mon.* **1977**, *3*, 5–7.
3. Lei, L.; Sun, J.S.; Wei, D. Distinguishing the Category of the Summer Convective Weather by Sounding Data in Beijing. *J. Meteorol. Mon.* **2011**, *37*, 136–141.
4. Wang, X.F.; Ding, Y.H. Study on Method of short-range Forecast of severe convective weather in Beijing Area. *J. Chin. J. Atmos. Sci.* **1994**, *18*, 173–183.
5. Chen, M.; Fan, S.Y.; Zheng, Z.F. The performance of the proximity sounding based on the BJ-RUC system and its preliminary implementation in the convective potential forecast. *J. Acta Meteorol. Sin.* **2011**, *69*, 181–194.
6. Tian, S.C.; Du, C.X. Effect of Merging of the Convective Cloud Clusters on Occurrence of Heavy Rainfall. *J. Chin. J. Atmos. Sci.* **1983**, *7*, 70–79.
7. Liao, X.N.; Yu, X.D.; Yu, B. Analysis on Infrequent Big Hail Event in Beijing Area. *J. Meteorol. Mon. Chin. J. Atmos. Sci.* **2008**, *34*, 12–19.
8. Ye, A.F.; Wu, Z.F.; Xiao, W. A study of application of cape in severe convective weather prediction. *J. Trop. Meteorol.* **2006**, *22*, 70–76.
9. Han, F.; Han, L.; Zhou, C.X. An experimental study of the short-time heavy rainfall event forecast based on ensemble learning and sounding data. *J. Appl. Meteorol. Sci.* **2021**, *32*, 188–199.
10. Zeng, M.J.; Wang, G.C.; Wu, H.Y. Study of the forecasting method for the classified severe convection weather based on a meso-scale numerical model. *J. Acta Meteorol. Sin.* **2015**, *73*, 868–882.
11. Wei, D.; Sun, J.S.; Lei, L. Reliability analysis of quantitative applications of sounding constructed from data detected by microwave radiometer and wind profiler. *J. Clim. Environ. Res.* **2011**, *16*, 697–706.
12. Liu, H.Y.; Xue, J.S.; Shen, T.L. Study on sounding balloon drifting and its impact on numerical predictions. *J. Appl. Meteorol. Sci.* **2005**, *16*, 518–526.
13. Zheng, L.J. *Diagnostic Analysis and Numerical Simulation of Meso Scale Synoptic System*; Meteorological Press: Beijing, China, 1989.
14. Cao, X.Z.; Xia, Y.C.; Luo, H.W. Technical Development and Prospect of Meteorological Sounding Observation. *J. Adv. Meteorol. Sci. Technol.* **2022**, *12*, 27–36.
15. Gao, T.; Guo, R.; Liu, Z.Y. Analysis of Dropsonde Observation Data of High-Altitude Large UAV. *J. Nat. Sci. J. Hainan Univ.* **2022**, *11*, 1–10.
16. Wei, Y.H.; Wang, Y.C.; Zhu, L.L. Confidence and Characteristics of Short-Duration Heavy Rainfall Environmental Parameters Based on Merging Data in Tianjin. *J. Desert Oasis Meteorol.* **2020**, *14*, 84–91.
17. Tian, F.Y.; Zheng, Y.G.; Zhang, T. Sensitivity analysis of short-duration heavy rainfall related diagnostic parameters with point-area verification. *J. Appl. Meteorol. Sci.* **2015**, *26*, 385–396.
18. John, X.Y.; Yong-Keun, L.; Christopher, G. Atmospheric humidity and temperature sounding from the CubeSat TROPICS mission: Early performance evaluation with MiRS. *J. Remote Sens. Environ.* **2023**, *287*, 113479.
19. Song, C.; Yin, Q. Research on vertical spatial characteristic of satellite infrared hyperspectral atmospheric sounding data. *J. Res. Artic.* **2022**, *2*, 265–276. [[CrossRef](#)]
20. Tan, H.; Huang, M.C.; Nong, M.S. Comparative Verification of sounding Data of Strong Convective Processes Based on FY-4A Temperature and Humidity Profiles. *J. Meteorol. Sci. Technol.* **2023**, *51*, 1–12.
21. Gao, T.; Guo, R.; Liu, Z.Y. Analysis of Dropsonde Observation Data of High-Altitude Large UAV. Inspection of FY-3D Satellite Temperature Data Based on Horizontal Drift Round-trip Sounding Data. *J. Appl. Meteorol. Sci.* **2023**, *34*, 52–64.
22. Kong, F.C.; Li, J.B.; Wang, Y. Analysis on atmospheric profiles retrieved by microwave radiometer at genting venue of Beijing Olympic Winter Games. *J. Meteorol. Mon.* **2021**, *47*, 1062–1072.



23. Chen, S.C.; Li, X.B.; Cui, M. Error analysis of detection data of microwave radiometer and wind profile radar under different weather conditions. *J. Meteorol. Environ.* **2021**, *31*, 67–72.
24. Xu, G.R.; Cui, C.G.; Zhou, Z.M. Atmospheric boundary layer heights estimated from radiosonde observations in the Qinghai-Tibet Plateau and its downstream areas. *J. Torrential Rain Disasters* **2014**, *33*, 217–227.
25. Liu, H.Y.; Li, J.; Cao, X.Y. Characteristics of the atmosphere remote sensed by the ground-based 12-channel radiometer. *J. Remote Sens. Technol. Appl.* **2007**, *22*, 222–229.
26. Westwater, E.R.; Han, Y.; Irisov, V.G. Remote sensing of boundary layer temperature profiles by a scanning 5-mm microwave radiometer and RASS: Comparison experiments. *J. Atmos. Ocean. Technol.* **1999**, *16*, 805–818. [[CrossRef](#)]
27. Lin, X.M.; Wei, Y.H.; Chen, H. The effect assessment of wind field inversion based on WPR in precipitation. *J. Appl. Meteorol.* **2020**, *31*, 361–372.
28. He, P. *Phased Array Wind Profile Radar*; Meteorological Press: Beijing, China, 2020.
29. Stanley, G.B.; Barry, E.S.; Eduard, J.S. The value of wind profiler data in US weather forecasting. *J. Bull. Am. Meteorol. Soc.* **2004**, *85*, 1871–1886.
30. He, P. *Foundation of Power Spectrum Estimation*; Meteorological Press: Beijing, China, 2015.
31. Dong, L.P.; Wu, L.; Wang, L. Preliminary comparison research of the Wind Profile Radar network data. *J. Meteorol. Mon.* **2014**, *40*, 1145–1151.
32. Qu, Q.N.; Sheng, C.Y.; Sun, Q. Comparison of horizontal wind between Wind Profile Radar and L Band Sounding Radar. *J. Arid. Meteorol.* **2016**, *34*, 1078–1086.
33. Furumoto, J.I.; Iwai, S.; Fujii, H.; Tsuda, T.; Xin, W.; Koike, T.; Bian, L. Estimation of humidity profiles with the L-band boundary layer radar-RASS measurement. *J. Meteorol. Soc. Jpn.* **2005**, *83*, 895–908. [[CrossRef](#)]
34. Furumoto, J.I.; Imura, S.; Tsuda, T.; Seko, H.; Tsuyuki, T.; Saito, K. The variational assimilation method for the retrieval of humidity profiles with the wind-profiling radar. *J. Atmos. Ocean. Technol.* **2007**, *24*, 1525–1545. [[CrossRef](#)]
35. Bianco, L.; Cimini, D.; Frank, S. Combining microwave radiometer and wind profiler radar measure for high-resolution atmospheric humidity profiling. *J. Atmos. Ocean. Technol.* **2005**, *22*, 949–965. [[CrossRef](#)]
36. Stankov, B.B.; Gossard, E.E.; Weber, B.L. Humidity gradient profiles from wind profiling radars using the NOAA/ETL advanced Signal Processing System (SPS). *J. Atmos. Ocean. Technol.* **2003**, *20*, 3–22. [[CrossRef](#)]
37. Imura, S.; Furumoto, J.; Tsuda, T. Estimation of humidity profiles by combining co-locate VHF and UHF wind-profiling radar observation. *J. Meteorol. Soc. Jpn.* **2007**, *85*, 301–319. [[CrossRef](#)]
38. Clayson, C.A.; Lakshmi, K. On turbulence and mixing in the free atmosphere inferred from high-resolution soundings. *J. Atmos. Ocean. Technol.* **2008**, *25*, 833–852. [[CrossRef](#)]
39. Sun, K.Y.; Ran, Z.; Wei, M. Preliminary estimation of specific humidity profiles with Wind Profile Radar. *J. Appl. Meteor. Sci.* **2013**, *24*, 407–415.
40. Cao, Y.J.; Liu, J.M.; Liang, H. Water vapor resource vertical stratification characteristics retrieved basing on the radiosonde datum. *J. Nat. Resour.* **2011**, *26*, 1603–1612.
41. Zhu, G.H.; Zhang, C.Y.; Weng, N.Q. Retrieve the atmospheric humidity profile from wind profile radar data. *J. Nat. Resour.* **2011**, *6*, 337–341.
42. Zhang, Q.C.; Gong, D.L.; Feng, J.J. Analysis and evaluation of retrieval products of RPG-HATPRO-G3 ground-based microwave radiometers. *J. Mar. Meteorol.* **2017**, *37*, 104–110.
43. Tang, R.M.; Cheng, Y.Y.; Ye, J.Y. The comparison of water vapor content retrieved by radiosonde, ground station and satellite data. *J. Meteorol. Sci.* **2010**, *30*, 373–377.
44. Lin, X.M.; He, P.; He, X.Y. A method to suppress the precipitation interference on horizontal wind of wind profile radar. *J. Appl. Meteor. Sci.* **2015**, *26*, 66–75.
45. Zhang, A.S. *Modern Meteorological Observation*; Peking University Press: Beijing, China, 2000.

**Disclaimer/Publisher’s Note:** The statements, opinions and data contained in all publications are solely those of the individual author(s) and contributor(s) and not of MDPI and/or the editor(s). MDPI and/or the editor(s) disclaim responsibility for any injury to people or property resulting from any ideas, methods, instructions or products referred to in the content.